Experimental and numerical study of the decomposition, product spectrum, and sooting properties of adamantane fuels

Ga-Un Jeong [a], Zhanhong Xiang [b], Sabari Kumar [c], Collin Hansen [c], Adri C.T. van Duin [a], Seonah Kim [c], Charles S. McEnally [b], Lisa D. Pfefferle [b], Yuan Xuan [a,*]

[a] *Department of Mechanical Engineering, The Pennsylvania State University, University Park, PA, 16802, USA*

[b] *Department of Chemical and Environmental Engineering, Yale University, New Haven, CT 06520, USA*

[c] *Department of Chemistry, Colorado State University, Fort Collins, CO 80523, USA*

Abstract

This work combined experimental measurements with two theoretical approaches, reactive Molecular Dynamics (MD) simulations and Quantum Mechanics (QM) calculations, to investigate the combustion and sooting properties of three adamantane fuels, adamantane (AD), 1,3-dimethyl-adamantane (DMAD), and 1-ethyl-adamantane (EAD). These fuels were selected since the adamantane fuel family can potentially be used as sustainable aviation fuels and comparing these fuels would reveal the effects of side chain on their combustion and sooting properties. We determined the bond dissociation energies of the three test fuels using QM calculations and found that the functionalized side chains have the weakest bonds and their presence only slightly affects the bond strength in the AD multi-cyclic core. We performed pyrolysis simulations for all three fuels using ReaxFF-based MD simulations and found that DMAD and EAD have higher decomposition rates than AD and also generate more high-molecular-weight products. For all three fuels, these large products were observed to contribute significantly to hydrocarbon growth processes, which lead to large soot nucleating

species and even soot-like structures. A higher yield of such soot nucleating compounds was found during the pyrolysis of DMAD and EAD than AD since the decomposition products of DMAD and EAD are more branched and those of AD have mostly straight chains. These theoretical analyses were supported by experimental measurements of yield-based sooting tendencies, which suggest that DMAD and EAD are sootier than AD and that all three fuels are sootier than standard alkane jet fuel surrogates but less sooty than jet fuel aromatic content.
Keywords: Molecular dynamics; Yield sooting index; Density function theory

*Corresponding author Email address: yux19@psu.edu (Yuan Xuan)

1. INTRODUCTION

Aviation is continually looking for Sustainable Aviation Fuels (SAF) comparable to conventional fuels due to the increasing demand for air traffic and significant emissions that cause climate change. The use of SAF derived from non-petroleum sources has the potential to decrease greenhouse gases and soot emissions, which mitigates the climate change impact of aviation by minimizing contrail formation [1] and the negative impacts on human health [2].

High-throughput synthetic chemistry techniques have been employed to produce advanced aviation fuels from petroleum with low melting point, high mass density and volumetric Net Heat of Combustion (NHOC), such as JP-10, which enables operation in cold climates and at high altitudes [3]. Given the favorable fuel properties of JP-10, many researchers have attempted to synthesize SAF from biomass with multicyclic structures similar to JP-10.

Adamantane (AD), which consists of four fused six-membered rings, was found to have good thermal stability and high NHOC [4], comparable to JP-10. It can be acquired from petroleum fractions [5] and its natural cracking [6] and synthesized from dicyclopentadiene [7], disseminated organic matter of rocks [8] or exhausted natural gas wells [9]. It has also been reported that it can be synthesized from tetrahydrodicyclopentadiene by Lewis-acid-catalyzed isomerization [7]. These properties collectively make adamantane an interesting candidate for aviation fuel. Nevertheless, its high melting point (269 °C) [3] makes it unsuitable to be a major component of liquid aviation fuels. Previous research has demonstrated that functionalizing AD with alkyl groups can dramatically reduce the melting point and viscosity, and increase fuel reactivity [3,4], making them suitable SAF candidates.

This work considered AD and two alkyl-substituted AD compounds, namely 1,3-dimethyl-adamantane (DMAD) and 1-ethyl-adamantane (EAD), as test fuels. AD was selected since it has the simplest fuel with a multi-cyclic structure. DMAD and EAD were selected for the simplicity of their side chains, and comparing the two isomers would reveal any potential side chain effects. The molecular structures of these fuels are shown in Fig. 1. Table 1 compares the melting point, mass density, and volumetric NHOC of AD, DMAD, EAD, JP-10, and *n*-dodecane (standard jet fuel surrogate component). It can be found that the multi-cyclic core ensures high density and volumetric NHOC for AD, DMAD, and EAD, comparable to jet fuels and their surrogate components, while the alkyl chains in DMAD and EAD provide low melting points, making them suitable for aviation applications.

While there is extensive experimental and theoretical literature on the synthesis and property quantification of AD fuels, research focusing on their combustion and emission characteristics is very limited. Harrison *et al.* [4] synthesized three different alkyl-substituted diamondoid fuels (1-ethyl-3-methyl adamantane, 1-propyladamantane, and C_{13}-C_{15} alkyl

diamondoids), and measured their mass density, freezing point, volumetric NHOC, and cetane number. Ma *et al.* [10] theoretically explored the side chain and isomer effects on the properties of 170 AD fuels, such as mass density, net heat value, specific impulse, and thermal and oxidation stability. Qin *et al.* [11] investigated the thermal stability of DMAD and hypothesized a DMAD thermal decomposition mechanism based on the component analysis of major gaseous products and liquid residues during pyrolysis. Al Zaabi *et al.* [2] observed strong synergistic soot suppression effects when AD was mixed into diesel. Despite these previous studies, there is still a significant lack of understanding of AD's combustion and emission characteristics and functionalized AD fuels under engine-relevant conditions.

In this work, we combined experimental measurements and theoretical approaches (quantum mechanics calculations and reactive Molecular Dynamics (MD) simulations) to reveal the combustion characteristics of AD, DAMD, and EAD. Specifically, we analyzed the bond strength of these fuels, their decomposition rates and pathways, major product distributions, and sooting tendencies. This approach aims to evaluate promising candidates for advancing the aviation industry and to enhance our understanding of alternative fuels that meet future environmental and performance requirements.

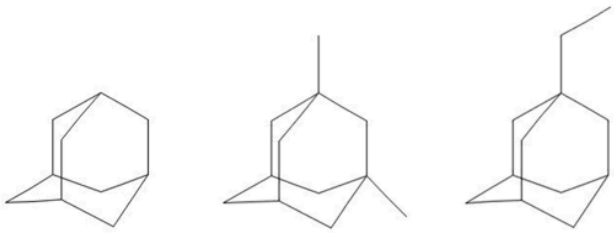

(a) (b) (c)

Figure 1. Molecular structures of the test fuels, (a) AD, (b) DMAD, and (c) EAD.

Table 1. Key fuel properties of AD, DMAD, EAD, JP-10, and n-dodecane.

	Melting point (°C)	Mass density (g/mL)	Volumetric NHOC (MJ/L)
JP-10	-79 [3]	0.94 [3]	39.4 [3]
n-dodecane	-9.55 [12]	0.75 [12]	34.6 [13]
AD	269 [3]	1.07 [14]	45.4 [15]
DMAD	-28.15 [16]	0.90 [16]	37.9 [4]
EAD	-24 [3]	0.95 [3]	40.2 [3]

2. METHODOLOGY

2.1. Quantum mechanics calculations

Quantum mechanics calculations were performed using Density Functional Theory (DFT) to determine the Bond Dissociation Energies (BDE) of the three test fuels. Initial conformers for the starting fuels and the ring-opened structures were generated, with their energy minimized using the MMFF94 forcefield [17]. The obtained conformer geometries were used as inputs for DFT optimization using the M06-2X functional [18] and def2TZVP basis set [19], as implemented in Gaussian16 [20]. This combination was selected based on the results of prior benchmarking studies, notably that performed by St. John et. al [21] and Mardirossian and Head-Gordon [22]. All calculations were performed as triplets for all diradical species, as benchmarking results [21] show that the triplet enthalpy is consistently lower than that of the singlet. BDEs were calculated by subtracting the formation enthalpy of the starting fuel structure from that of the resultant fragment(s) due to bond cleavage. The obtained single point energies were subjected to quasi-harmonic corrections using the Goodvibes [23] software package.

2.2 ReaxFF reactive MD simulations

High temperature pyrolysis of the three fuels was simulated using ReaxFF-based reactive MD. ReaxFF describes reactive events through a bond-order concept. The bond order is calculated directly from interatomic distance and updated at every iteration, which captures bond formation and breaking. The total energy of a system consists of many-body empirical potential *terms*. ReaxFF calculates the energy of each atom in the system using the following equation:

$$E_{system} = E_{bond} + E_{over} + E_{under} + E_{lp} + E_{val} + E_{tor} + E_{vdWaals} + E_{Coulomb} \quad (1)$$

where E_{bond} (bond energy), E_{over} (over-coordination penalty energy), E_{under} (under-coordination penalty energy), E_{lp} (lone pair energy), E_{val} (valence angle energy), and E_{tor} (torsion angle energy) are bond-order-dependent terms. $E_{vdWaals}$ (van der Waals energy) and $E_{Coulomb}$ (Coulomb energy) are non-bonded terms. ReaxFF employs Morse potential for the van der Waals interactions and the Electronegativity Equalization Method (EEM) for Coulomb interactions. More detailed descriptions of the ReaxFF methodology can be found in previous publications [24,25].

We followed a well-established ReaxFF-based simulation framework [26–28] to study the pyrolysis of AD, DMAD, and EAD. For the pyrolysis simulation of each fuel, 40 fuel molecules in their energy minimized structures were randomly placed in a 3D-periodic box of appropriate size to reach the desired density of 0.2 kg/dm^3. We did not consider oxygen because in a typical non-premixed flame (e.g., the flame discussed in Section 2.3), fuel pyrolysis occurs under highly fuel rich conditions. The density of 0.2 kg/dm^3 at this temperature condition leads to pressures much higher than those in practical combustion devices, since ReaxFF simulations typically need relatively high pressures and temperatures to accelerate the reaction dynamics, and the higher pressure does not affect the type of reactions that are occurring [29].

The prepared system was equilibrated at 1500 K for 2.5 ps through NVT-MD simulation, where the number of atoms (N), volume (V), and temperature (T) were kept constant. This step was carried out to stabilize the randomly arranged molecules without any chemical reaction occurring. After equilibration, additional NVT simulations were performed at 2500 K with a time step of 0.1 fs to observe fuel pyrolysis. These simulations were performed for 3 ns to ensure all fuels could decompose. We performed 3 statistically independent simulations for each fuel with three different initial configurations and ensemble-averaged the results to minimize statistical noise. All ReaxFF results reported in this work were based on ensemble-averaged data from the three NVT-MD simulations. The C/H/O force field [27] that was previously developed and validated was used in all ReaxFF simulations. The same force field has been used in previous studies for similar simulations with jet fuels, fuel surrogates, and fuel additives [28,30]. We used an in-house reaction analysis code to identify all reactions during MD simulations. This code is designed with the assumption that the recognition of a species with a different chemical formula implies the occurrence of a reaction event[28]. The ReaxFF simulation results were used to analyze the initial decomposition, product spectrum, and hydrocarbon growth of the three test fuels.

2.3 Sooting tendency measurements

Sooting tendencies were measured using a yield-based approach we developed previously [31]. The procedure used in this study is described in [32]. It consists of three steps: (1) we sequentially doped 1000 ppm (1000 μmol/mol) of n-heptane (H), toluene (TOL), and each test sample (TS) into the fuel of a base methane/air flame; (2) we measured the maximum soot concentration in each flame with line-of-sight spectral radiance (LSSR); and (3) we rescaled the results into a yield sooting index (YSI) defined as:

158 $$YSI_{TS} = (YSI_{TOL} - YSI_H) \times \frac{LSSR_{TS} - LSSR_H}{LSSR_{TOL} - LSSR_H} + YSI_H \quad (2)$$

159 This rescaling factors out sources of systematic uncertainty such as methane errors and air
160 flowrate errors. Furthermore, it allows the new results to be compared quantitatively with a
161 database that containing measured YSIs for hundreds of organic compounds [33]. The
162 parameters YSI_{TOL} and YSI_H are constants that define the YSI scale; their values, 170.9 and
163 36.0, were taken from the database so that the newly measured YSIs would be on the same
164 scale for a direct comparison.

165 Supplemental Information (SI) A lists the sources and purities of the reactants. SI B shows
166 a schematic diagram of the LSSR apparatus and SI C gives details of the specific burner
167 [34,35]. The liquid test fuels were injected into the gas-phase CH_4/N_2 fuel mixture with a
168 syringe pump. SI D lists the liquid-phase flow rates corresponding to 1000 ppm in the gas-
169 phase for each mixture, and the property values [36] that were used to calculate them. Each
170 test fuel was injected for 600 s, and the LSSR signal was averaged from 300 to 600 s; SI E
171 shows that the initial 300 s is adequate for the test fuel to equilibrate with the walls of the fuel
172 line and burner. The fuel lines were heated to 90 °C and above, and the burner was heated to
173 170 °C. SI F shows that the LSSR signals of DMAD increased linearly with the test fuel mole
174 fraction, which experimentally confirms that the test fuel was not condensing in the fuel
175 delivery system. Iso-octane was included in each measurement set as an internal standard; SI
176 G shows that the values were consistent over time and agreed with previous measurements
177 [33].

178 Each YSI was measured three times and then averaged. The random uncertainty is
179 estimated to be ±2% based on the standard deviation of the measured values for the internal
180 standard. The systematic uncertainty in YSI is estimated to be ±1%, mainly due to uncertainty
181 in the ratio of the mass densities between species. There is an additional uncertainty when

comparing the new measurements with the earlier measurements in [33], which we estimate to add ±2% based on the measured values of the internal standard versus its value in [33]. Overall, we estimate that the uncertainty in the measured YSI is ±5% or ±5.0, whichever is larger.

3. RESULTS AND DISCUSSION

3.1 Bond Dissociation Energy (BDE) analysis

The BDEs of AD, DMAD, and EAD were determined using DFT-based quantum mechanics calculations, as shown in SI I. These BDE calculations would reveal how the alkyl side chains might alter the initial combustion reactions; the bonds with the weakest BDE can be assumed to be most easily pyrolytically cleaved during combustion. It was observed that the BDEs for all bonds in AD are the same, due to the symmetry of the AD molecular structure. The methyl groups in DMAD slightly change the BDEs of the bonds in the multi-cyclic AD core of the molecule by approximately ±10%. The C-C bonds connecting the methyl groups to the AD core were found to have the lowest BDEs, which suggests that side chain dissociation would likely be a dominant initial decomposition pathway for DMAD. Similarly, the ethyl group in EAD only changes the BDEs of the bonds in the multi-cyclic AD core of the molecule by approximately ±7%. The two C-C bonds in the ethyl group were found to be significantly weaker than all the bonds in the AD core, which suggests that side chain dissociation would be preferred for EAD decomposition as well.

3.2 Fuel decomposition

Fuel reactivity at combustion temperatures strongly affects the location of combustion events and combustion efficiency. The reactivity of AD, DMAD, and EAD was quantified in

Fig. 2, where ensemble-averaged time histories of the number of fuel molecules extracted from ReaxFF MD pyrolysis simulations were shown. It was observed that AD, DMAD, and EAD were fully consumed after approximately 0.19, 0.20, and 0.15 ns, respectively. This suggests that EAD has a slightly higher decomposition rate than AD and DMAD, which have similar decomposition rates at this temperature. This is consistent with the BDE calculations reported in Section 3.2, where the ethyl chain in EAD was found to have the lowest BDE among all the bonds in the three fuels.

The major decomposition pathways for the three fuels investigated were also extracted from ReaxFF simulations, as shown in Table 2 (minor pathways with less than 5% contribution were not shown). Table 2 shows the integrated data of decomposition pathways originating from fuel molecules and fuel radicals, considering hydrogen abstraction followed by radical dissociation or isomerization. In addition, Figure 3 illustrates the reaction pathways for the decomposition and sooting of the three adamantane fuels, highlighting the differences between them. The most preferred decomposition channel for AD is R1 (65%), which leads to forming of straight-chain allyl radicals, C_7H_{11} and C_3H_5. Similarly, all other major AD decomposition pathways also lead to allyl radicals with mostly straight chains and low levels of branching. For DMAD and EAD, the most preferred decomposition pathways were identified to be the separation of side chains (R1 in both cases), consistent with the BDE calculations reported in Section 3.2. However, the dominance of these reactions is not strong, since other reaction channels were also found to contribute significantly to fuel decomposition. The adamantane radical resulting from Reactions R1 for DMAD and EAD were observed to decompose further following similar pathways as AD. Due to fuel side chains, other decomposition pathways of DMAD and EAD typically lead to branched allyl radicals. For instance, the C_8H_{13} and C_4H_7 radicals formed by R2 for DMAD are both branched, containing

a methyl group from the original fuel molecule. The C_9H_{15} radical formed by R2 for EAD is branched and contains the ethyl side chain from EAD. In particular, the two side chains in DMAD lead to the formation of radicals with higher levels of branching compared to EAD where a side chain is concentrated on one side of the AD core. Given that branched alkanes and alkenes are generally thermodynamically more stable than their linear isomers [37], the initial products formed from AD pyrolysis would likely further decompose into smaller fragments, whereas the initial products formed from DMAD and EAD pyrolysis would have a higher chance of forming larger hydrocarbons, potentially leading to higher soot propensity, as discussed in the following section.

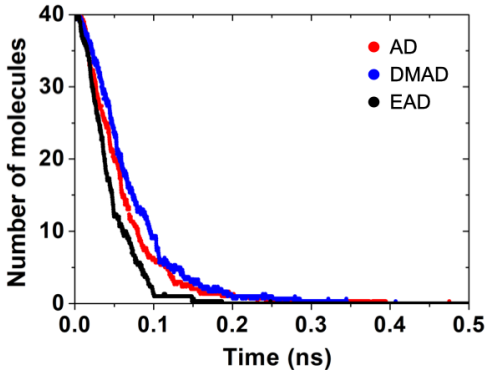

Figure 2. Time evolution of the fuel molecules extracted from ReaxFF MD simulations.

248 **Table 2.** Major initial decomposition reactions of AD, DMAD, and EAD extracted from
249 ReaxFF pyrolysis simulations at 2500 K.

Fuel	Decomposition pathway	Contribution
AD ($C_{10}H_{16}$)	(R1) $C_7H_{11} + C_3H_5$	65%
	(R2) $C_5H_8 + C_5H_8$	19%
	(R3) $C_8H_{13} + C_2H_3$	14%
	(R4) $C_6H_9 + C_4H_7$	8%
DMAD ($C_{12}H_{20}$)	(R1) $C_{11}H_{17} + CH_3$	28%
	(R2) $C_8H_{13} + C_4H_7$	25%
	(R3) $C_9H_{15} + C_3H_5$	22%
	(R4) $C_7H_{12} + C_5H_8$	10%
EAD ($C_{12}H_{20}$)	(R1) $C_{10}H_{15} + C_2H_5$	31%
	(R2) $C_9H_{15} + C_3H_5$	27%
	(R3) $C_7H_{12} + C_5H_8$	22%
	(R4) $C_{11}H_{17} + CH_3$	11%

250

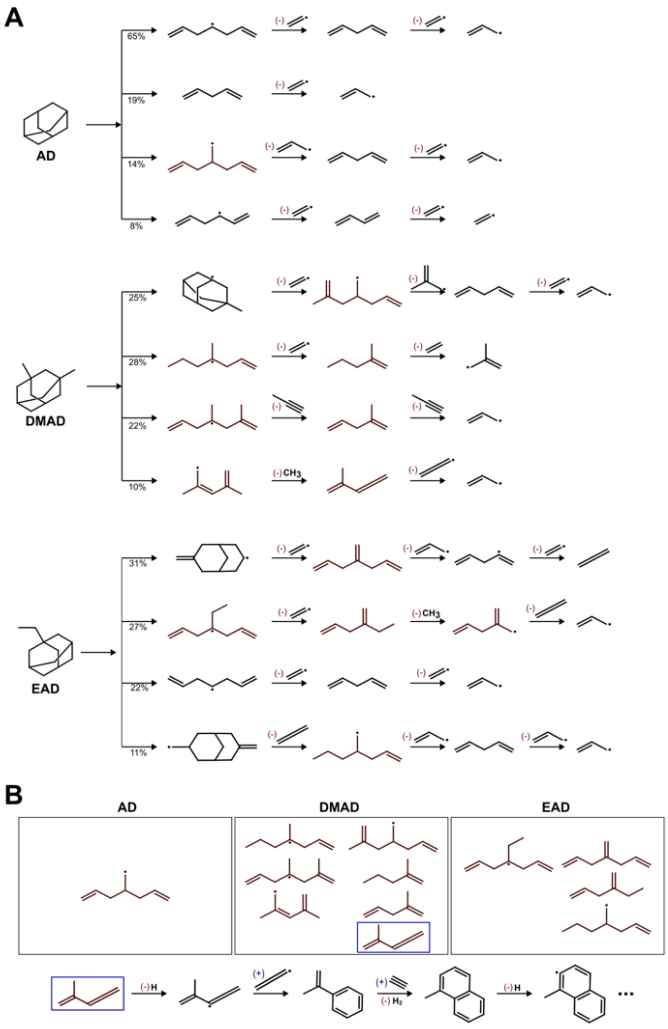

Figure 3. Panel A illustrates the decomposition pathways of three adamantane fuels: AD (adamantane), DMAD (1,3-dimethyl-adamantane), and EAD (1-ethyl-adamantane). The initial decomposition step is depicted, with the percentage contribution of each pathway provided. Following this step, the potential decomposition of intermediates into various radicals is shown. Panel B presents a table listing the branched intermediates generated from the decomposition of AD, DMAD, and EAD. Below the table, a specific branched intermediate structure from DMAD is highlighted, demonstrating its potential growth through

radical chain reactions. This process results in larger resonance-stabilized radicals, which can subsequently contribute to soot formation [38,39].

3.3 Product distribution

Figure 4 shows the ensemble-averaged time histories of major products formed during the pyrolysis of AD, DMAD, and EAD, extracted from ReaxFF MD simulations. Note that all compounds and radicals with the same number of carbon atoms are lumped together due to the large range of products generated. It is observed that all three fuels lead to the formation of not only small hydrocarbon fragments, such as C2 and C3 compounds, but also high-molecular-weight hydrocarbons, such as C5-C7. Most of these major products are formed rapidly within the first 0.2 ns of the simulations for all three fuels, which suggests that they directly result from the initial fuel decomposition reactions (listed in Table 2). Once formed, the number of all major products for all three fuels were found to slowly but constantly decrease throughout the simulation. This suggests that the high-molecular-weight products (C5-C7) do not further decompose into smaller fragments (C2-C3), but instead, may go through hydrocarbon growth pathways leading to soot precursors.

This behavior is different from what we observed previously for conventional jet fuels and fuel surrogates, such as *n*-dodecane and JP-10 [30], as well as for other bio-derived bi-cyclic fuels, such as dodeca-hydrobiphenylene ($C_{12}H_{20}$) and 1,1′-bi-cyclohexane ($C_{12}H_{22}$) [28]. These fuels contain similar numbers of carbon atoms as AD, DMAD, and EAD, but they form C2-C4 alkenes as the major products, without significant hydrocarbon growth. They also form low levels of high-molecular-weight hydrocarbons, which rapidly break down into smaller fragments. Based on this comparison, AD, DMAD, and EAD fuels would likely lead to higher soot production compared these aforementioned fuels.

By cross-comparing the product distributions from AD, DMAD, and EAD it was observed that AD and DMAD produce lower levels of C2 compounds compared to EAD, due to the EAD ethyl side chain separation reaction. DMAD and EAD produce more and larger high-molecular-weight hydrocarbons than AD, likely due to the presence of side chains and the more stable branched structures of their products. This implies that DMAD and EAD would lead to more pronounced hydrocarbon growth than AD.

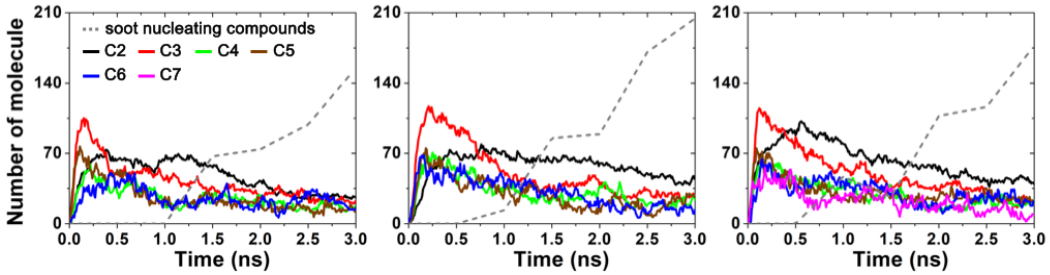

(a) (b) (c)

Figure 4. Time evolution of major pyrolysis products of (a) AD, (b) DMAD, and (c) EAD extracted from ReaxFF MD simulations.

3.4 Hydrocarbon growth

To better quantify the hydrocarbon growth process from the smaller C2-C7 products shown in Fig. 4, the entire hydrocarbon product spectrum was extracted at the end of the ReaxFF simulations (3 ns), as shown in Fig. 5 for all three fuels. Similar to Fig. 4, all compounds and radicals with the same number of carbon atoms are lumped into the one bin. It was observed that large amounts of highly unsaturated large hydrocarbons (> C20) are formed for all three fuels. Such compounds were not found in similar simulations from previous studies of jet fuels, fuel surrogates, [30], and bio-derived bi-cyclic fuel additives [28].

The molecular structures were extracted from ReaxFF simulations for three of such compounds formed from EAD pyrolysis, as shown in Fig. 6. Poly-cyclic structures were

observed in all three molecules, which demonstrates that they can be classified as soot precursors. Based on this observation, the highly unsaturated large hydrocarbon products that contain at least three inter-connected aromatic rings were highlighted in yellow in the entire product distribution for all three fuels shown in Fig. 5. We considered these compounds as soot precursors that can directly lead to chemical or physical nucleation to form soot [40]. This is a rather conservative cut-off, since some previous studies have considered naphthalene as the smallest Poly-cyclic Aromatic Hydrocarbon (PAH) that leads to soot nucleation [40]. At the end of the pyrolysis simulations, these compounds contain 30%, 51%, and 44% of the total number of carbon atoms in the system for AD, DMAD, and EAD, respectively. In addition, the dominant molecular structures of the low molecular weight products (≤ C5) from AD, DMAD, and EAD decomposition are the same and are provided in SI J. This result is expected, since the side chains primarily affect high molecular weight products.

The time-histories of the total number of carbon atoms contained in the "soot nucleating compounds" (yellow-highlighted bins in Fig. 5 all combined) were extracted from ReaxFF simulations for all three fuels, as shown by the red dash line in Fig. 4. It was observed that soot nucleating compounds start to form earlier for DMAD and EAD compared to AD. In addition, DMAD and EAD pyrolysis lead to a higher yield of these compounds compared to AD. These differences are likely due to the branched structures found in the direct pyrolysis products for DMAD and EAD, which are more stable and prone to hydrocarbon growth.

These results imply that AD, DMAD, and EAD would have higher sooting tendencies than JP-10, n-dodecane, and bi-cyclic alkanes (previously investigated using ReaxFF [28,30]), and that DMAD and EAD would have similar sooting tendencies, higher than that of AD.

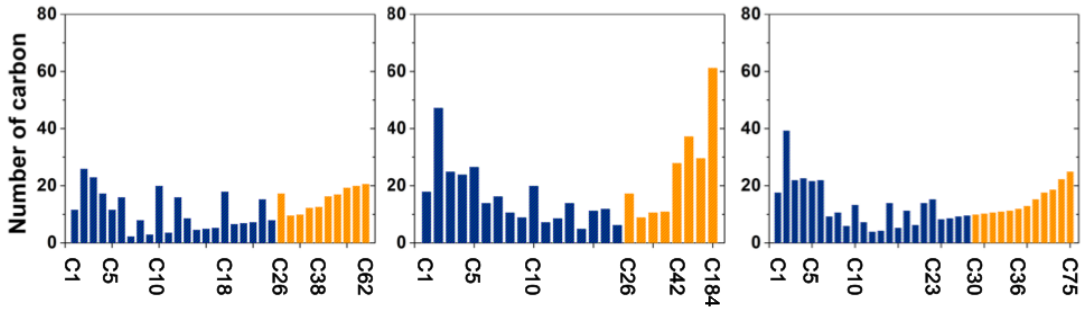

(a) (b) (c)

Figure 5. Product spectrum of (a) AD, (b) DMAD, and (c) EAD extracted at the end of the ReaxFF pyrolysis simulations.

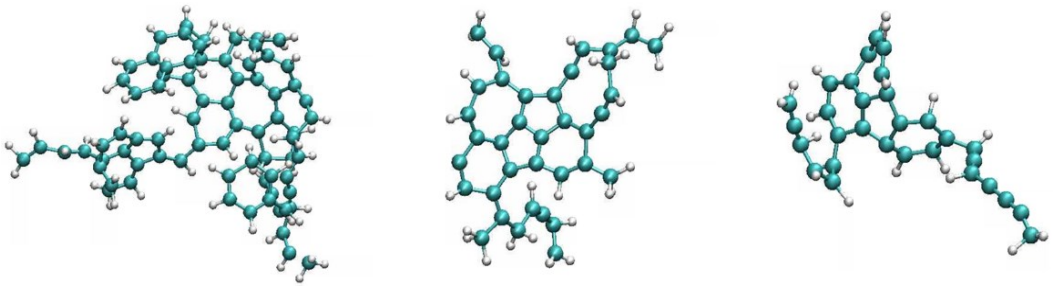

(a) (b) (c)

Figure 6. Molecular structures of large highly-unsaturated hydrocarbons (a) $C_{75}H_{57}$, (b) $C_{36}H_{26}$, and (c) $C_{30}H_{19}$ extracted at the end of the ReaxFF pyrolysis simulations for EAD.

3.5 Experimental sooting tendency measurements

The observations made above based on the analysis of ReaxFF-based MD simulation results were supported by and in agreement with actual sooting tendency measurements. We measured yield-based sooting tendencies (i.e., YSIs) for AD, DMAD, and EAD, which are listed in Table 3. This table also lists the YSIs measured previously [33] for the set of

compounds proposed in [41] as a palette for formulating jet fuel surrogates. These values indicate how the adamantanes compare to other jet-fuel-relevant hydrocarbons.

DMAD and EAD are liquids at room temperature, so their YSIs could be measured with the normal procedure. In contrast, AD is a solid with a melting point of 270 °C [42] and it could not be injected into the fuel mixture as a pure compound. Instead, we dissolved AD into *n*-heptane (H) and measured the YSIs of the resulting liquid mixtures (YSI_{mix}). The mixtures had AD mole fractions (x_{AD}) of 0.02, 0.04, 0.06, and 0.08; higher values could not be achieved due to the solubility limit.

Figure 7 shows the results. YSI_{mix} increases linearly as x_{AD} increases, at a slope corresponding to $YSI_{AD} = 174$. We estimate the uncertainty in this value as ±20 YSI units based on its sensitivity to the details of the analysis. This uncertainty is more significant than normal YSI measurements since the AD is responsible for only one-third or less of the soot in these flames.

The only previous study of adamantane sooting tendencies observed a strong synergistic soot suppression effect when AD was mixed into diesel fuel [2]. The Smoke Point (SP) was 18 mm for pure diesel, increased to 23 and 29 mm with $x_{AD} = 0.01$ and 0.0675, and then decreased to 23 mm for $x_{AD} = 0.08$. (SP is a threshold-based sooting tendency where higher values correspond to less sooty fuels [43].) In contrast, the data in Fig. 7 follows a linear blending rule with no synergistic effect.

The ASTM specifications for Jet A [44] require SP ≥ 18 mm. We showed in earlier work that YSI and 1/SP are correlated, such that a Derived Smoke Point (DSP) can be calculated from a measured YSI. Table 3 lists DSPs calculated in SI H for the adamantanes and the other jet fuel components. All the adamantanes have DSP < 18 mm, so they would not be suitable as pure Jet A fuels. However, their DSPs are significantly higher than the aromatic

components (12.9 to 13.9 vs. 3.1 to 9.0), so to the extent that they can replace the aromatics in jet fuel, they will likely reduce soot emissions.

Table 3. YSIs of adamantanes measured in this study, YSIs measured earlier for some other jet fuel compounds [33], and Derived Smoke Points (DSPs) calculated from the YSIs (see SI H).

Name	YSI	DSP
AD	174 ± 20	13.9
DMAD	235 ± 12	12.3
EAD	225 ± 11	12.9
n-decane	54 ± 5	100.2
n-dodecane	67 ± 5	91.2
n-tetradecane	78 ± 5	90.1
isocetane	128 ± 6	45.5
methylcyclohexane	54 ± 5	47.3
n-butylcyclohexane	77 ± 5	47.0
1,2-xylene	200 ± 10	8.5
n-butylbenzene	245 ± 12	9.0
trimethylbenzene	311 ± 16	6.1
tetralin	336 ± 17	6.1
1-methylnaphthalene	649 ± 32	3.1

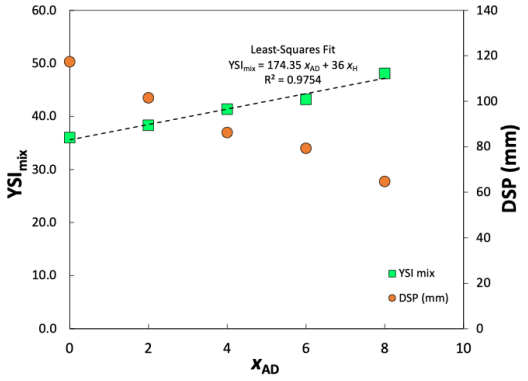

Figure 7. YSIs measured for mixtures of *n*-heptane (H) with AD. The error bars indicate the ±2% random uncertainty. The Derived Smoking Point (DSP) data is also provided for reference.

4. CONCLUSIONS

This study used experimental measurements, DFT-based quantum mechanics calculations, and ReaxFF-based MD simulations to investigate the decomposition rates and reaction pathways, product distributions, and sooting tendencies of three adamantane fuels, AD, DMAD, and EAD. These fuels were found to have high decomposition rates and yield significant amounts of high-molecular-weight products. These products go through pronounced hydrocarbon growth processes leading to multi-ring aromatic species with even soot-like structures, which have relatively high sooting tendencies, as confirmed by experimental measurements. Therefore, adamantane fuels with functionalized side chains would not be suitable as pure jet fuels, but can potentially replace the aromatic content in jet fuels, to reduce soot emissions.

The presence of the side chains was found to have significant effects on DMAD and EAD decomposition since side chain separation was the dominant initial pathway. The side chains also make the decomposition products of DMAD and EAD more branched than those of AD.

Therefore, more hydrocarbon growth was found following DMAD and EAD decomposition, compared to AD. For these reasons, DMAD and EAD have higher sooting tendencies than AD, in agreement with current measurements.

Declaration of competing interest

The authors declare that they have no known competing financial interests or personal relationships that could have appeared to influence the work reported in this paper.

Acknowledgments

This work was supported by the U.S. National Science Foundation award CBET 2210894. The ReaxFF MD simulations were performed on the Roar supercomputer managed by the Penn State Institute for Computational and Data Sciences. CSU work was supported by the Colorado State University startup funds for PI (Seonah Kim) and the computer time was provided by the NSF Extreme Science and Engineering Discovery Environment (XSEDE, now ACCESS), Grant no. TG-CHE210034. The authors appreciate contributions from Mehmet Acikel, Muhammed Oruc, Zhengrong Qian, David Wang, and Vivian Whoriskey.

Supplementary material

Supplementary material associated with this article can be found, in the online version, at a DOI link to be filled in later.

References

[1] Dray L, Schäfer AW, Grobler C, Falter C, Allroggen F, Stettler MEJ, et al. Cost and emissions pathways towards net-zero climate impacts in aviation. Nat Clim Chang 2022;12:956–62. https://doi.org/10.1038/s41558-022-01485-4.

[2] Zaabi A Al, Raj A, Elkadi M, Anjum D, Li L, George A, et al. Effects of the addition of a high energy density fuel, adamantane to diesel on its cetane number, sooting propensity, and soot nanostructural properties. Cleaner Chemical Engineering 2022;2:100008. https://doi.org/10.1016/j.clce.2022.100008.

[3] Harvey BG, Harrison KW, Davis MC, Chafin AP, Baca J, Merriman WW. Molecular Design and Characterization of High-Cetane Alkyl Diamondoid Fuels. Energy and Fuels 2016;30:10171–8. https://doi.org/10.1021/acs.energyfuels.6b01865.

[4] Harrison KW, Rosenkoetter KE, Harvey BG. High Density Alkyl Diamondoid Fuels Synthesized by Catalytic Cracking of Alkanes in the Presence of Adamantane. Energy and Fuels 2018;32:7786–91. https://doi.org/10.1021/acs.energyfuels.8b00792.

[5] Fort RC, Schleyer PVR. Adamantane: consequences of the diamondoid structure. Chem Rev 1964;64:277–300.

[6] Dahl J, Moldowan J, Peters K, Claypool G, Rooney M, Michael G, et al. Diamondoid hydrocarbons as indicators of natural oil cracking. Nature 1999;399:54–7.

[7] Schleyer PVR. A simple preparation of adamantane. J Am Chem Soc 1957;79:3292.

[8] Giruts M V., Rusinova G V., Gordadze GN. Generation of adamantanes and diamantanes by thermal cracking of high-molecular-mass saturated fractions of crude oils of different genotypes. Petroleum Chemistry 2006;46:225–36. https://doi.org/10.1134/S0965544106040025.

[9] Chung HS, Chen GSH, Kremer RA, Boulton JR, Burdette GW. Recent developments in high-energy density liquid hydrocarbon fuels. Energy and Fuels 1999;13:641–9. https://doi.org/10.1021/ef980195k.

[10] Ma J, Yin L, Ling L, Zhang R, Yan G, Wang J, et al. The prediction and assessment of properties for high energy density fuel – Adamantane derivatives: The combined DFT and molecular dynamics simulation. Fuel 2023;343. https://doi.org/10.1016/j.fuel.2023.127975.

[11] Qin X, Yue L, Wu J, Guo Y, Xu L, Fang W. Thermal stability and decomposition kinetics of 1,3-dimethyladamantane. Energy and Fuels 2014;28:6210–20. https://doi.org/10.1021/ef5011644.

[12] Haynes WM. CRC Handbook of Chemistry and Physics. 95th Edition. Boca Raton: FL: CRC Press LLC; 2014.

[13] NIST Chemistry WebBook, SRD 69 n.d. https://webbook.nist.gov/cgi/cbook.cgi?ID=C112403&Mask=FFF (accessed December 4, 2023).

[14] Haynes WM. CRC Handbook of Chemistry and Physics. 97th ed. CRC Press; 2016.

[15] Kabo GY, Kazarina ZA, Stepurko EN, Blokhin A V. Energy Density of Adamantane-Containing Hydrocarbons in Condensed Phases. Petroleum Chemistry 2022;62:499–505. https://doi.org/10.1134/S0965544122020219.

[16] Qin X, Cao X, Guo Y, Xu L, Hu S, Fang W. Density, viscosity, surface tension, and refractive index for binary mixtures of 1,3-dimethyladamantane with four C10 alkanes. J Chem Eng Data 2014;59:775–83. https://doi.org/10.1021/je4008926.

[17] Halgren TA. Merck molecular force field. V. Extension of MMFF94 using experimental data, additional computational data, and empirical rules. J Comput Chem 1996;17:616–614.

[18] Zhao Y, Truhlar DG. The M06 suite of density functionals for main group thermochemistry, thermochemical kinetics, noncovalent interactions, excited states, and transition elements: Two new functionals and systematic testing of four M06-class functionals and 12 other functionals. Theor Chem Acc 2008;120:215–41. https://doi.org/10.1007/s00214-007-0310-x.

[19] Weigend F. Accurate Coulomb-fitting basis sets for H to Rn. Physical Chemistry Chemical Physics 2006;8:1057–65. https://doi.org/10.1039/b515623h.

[20] Frisch MJ, Trucks GW, Schlegel HB, Scuseria GE, Robb MA, Cheeseman JR, et al. Gaussian 16, Revision C.01. Gaussian, Inc, Wallingford CT 2016.

[21] St. John PC, Guan Y, Kim Y, Kim S, Paton RS. Prediction of organic homolytic bond dissociation enthalpies at near chemical accuracy with sub-second computational cost. Nat Commun 2020;11:2328. https://doi.org/10.1038/s41467-020-16201-z.

[22] Mardirossian N, Head-Gordon M. How Accurate Are the Minnesota Density Functionals for Noncovalent Interactions, Isomerization Energies, Thermochemistry, and Barrier Heights Involving Molecules Composed of Main-Group Elements? J Chem Theory Comput 2016;12:4303–25. https://doi.org/10.1021/acs.jctc.6b00637.

[23] Luchini G, Alegre-Requena J V., Funes-Ardoiz I, Paton RS. GoodVibes: automated thermochemistry for heterogeneous computational chemistry data. F1000Res 2020;9:291. https://doi.org/10.12688/f1000research.22758.1.

[24] Van Duin ACT, Dasgupta S, Lorant F, Goddard WA. ReaxFF: A reactive force field for hydrocarbons. Journal of Physical Chemistry A 2001;105:9396–409. https://doi.org/10.1021/jp004368u.

[25] Senftle TP, Hong S, Islam MM, Kylasa SB, Zheng Y, Shin YK, et al. The ReaxFF reactive force-field: Development, applications and future directions. NPJ Comput Mater 2016;2. https://doi.org/10.1038/npjcompumats.2015.11.

[26] Chenoweth K, Van Duin ACT, Goddard WA. ReaxFF reactive force field for molecular dynamics simulations of hydrocarbon oxidation. Journal of Physical Chemistry A 2008;112:1040–53. https://doi.org/10.1021/jp709896w.

[27] Ashraf C, Van Duin ACT. Extension of the ReaxFF Combustion Force Field toward Syngas Combustion and Initial Oxidation Kinetics. Journal of Physical Chemistry A 2017;121:1051–68. https://doi.org/10.1021/acs.jpca.6b12429.

[28] Lele A, Kwon H, Ganeshan K, Xuan Y, van Duin ACT. ReaxFF molecular dynamics study on pyrolysis of bicyclic compounds for aviation fuel. Fuel 2021;297. https://doi.org/10.1016/j.fuel.2021.120724.

[29] Krep L, Kopp WA, Kröger LC, Döntgen M, Leonhard K. Exploring the Chemistry of Low-Temperature Ignition by Pressure-Accelerated Dynamics. ChemSystemsChem 2020;2. https://doi.org/10.1002/syst.201900043.

[30] Ashraf C, Shabnam S, Jain A, Xuan Y, van Duin ACT. Pyrolysis of binary fuel mixtures at supercritical conditions: A ReaxFF molecular dynamics study. Fuel 2019;235:194–207. https://doi.org/10.1016/j.fuel.2018.07.077.

[31] McEnally CS, Pfefferle LD. Improved sooting tendency measurements for aromatic hydrocarbons and their implications for naphthalene formation pathways. Combust Flame 2007;148:210–22. https://doi.org/10.1016/j.combustflame.2006.11.003.

[32] Zhu J, Alegre-Requena J V, Cherry P, Curtis D, Harvey BG, Jabed MA, et al. Sooting tendencies of terpenes and hydrogenated terpenes as sustainable transportation biofuels. Proceedings of the Combustion Institute 2023;39:877–87.

[33] McEnally CS, Das DD, Pfefferle LD. Yield sooting index database volume 2: Sooting tendencies of a wide range of fuel compounds on a unified scale. Harvard Dataverse 2017. https://doi.org/10.7910/DVN/7HGFT8.

[34] Franzelli B, Roussillo M, Scouflaire P, Bonnety J, Jalain R, Dormieux T, et al. Multi-diagnostic soot measurements in a laminar diffusion flame to assess the ISF database consistency. Proceedings of the Combustion Institute 2019;37:1355–63. https://doi.org/10.1016/j.proci.2018.05.062.

[35] J. Gau, D. Das, C. McEnally, D. Giassi, N. Kempema, M. Long. Yale Coflow Burner Information and CAD Drawings 2017. https://doi.org/10.6084/m9.figshare.5005007.v1.

[36] Mathieu D, Bouteloup R. Reliable and versatile model for the density of liquids based on additive volume increments. Ind Eng Chem Res 2016;55:12970–80. https://doi.org/10.1021/acs.iecr.6b03809.

[37] Ess DH, Liu S, De Proft F. Density functional steric analysis of linear and branched alkanes. Journal of Physical Chemistry A 2010;114:12952–7. https://doi.org/10.1021/jp108577g.

[38] Johansson KO, Head-Gordon MP, Schrader PE, Wilson KR, Michelsen HA. Resonance-stabilized hydrocarbon-radical chain reactions may explain soot inception and growth. Science (1979) 2018;361:997–1000.

[39] H. J. Singh, N. K. Gour. Recombination of propargyl radicals to form benzene: A computational study. Indian J Chem 2010;49B:1565–70.

[40] Shao C, Wang Q, Zhang W, Bennett A, Li Y, Guo J, et al. Elucidating the polycyclic aromatic hydrocarbons involved in soot inception. Commun Chem 2023;6. https://doi.org/10.1038/s42004-023-01017-x.

[41] Colket M, Edwards T, Williams S, Cernansky NP, Miller DL, Egolfopoulos F, et al. Development of an Experimental Database and Kinetic Models for Surrogate Jet Fuels AIAA 2007-770. In 45th AIAA Aerospace Sciences Meeting and Exhibit 2007;770.

[42] J.R. Rumble. CRC Handbook of Chemistry and Physics. 101st ed. http://hbcponline.com/faces/contents/ContentsSearch.xhtml; 2019.

[43] ASTM D1322-22 Standard Test Method for Smoke Point of Kerosene and Aviation Turbine Fuel. ASTM International 2022. https://doi.org/10.1520/D1322-22.

[44] ASTM D7566-23a Standard Specification for Aviation Turbine Fuel Containing Synthesized Hydrocarbons. ASTM International 2023. https://doi.org/10.1520/D7566-23A.